




Pattern of Cerebellar Atrophy in Friedreich's Ataxia—Using the SUIT Template

Tobias Lindig^{1,2}  · Benjamin Bender^{1,2} · Vinod J. Kumar² · Till-Karsten Hauser¹ · Wolfgang Grodd² · Bettina Brendel^{3,4} · Jennifer Just^{5,6} · Matthis Synofzik^{5,6} · Uwe Klöse¹ · Klaus Scheffler^{2,7} · Ulrike Ernemann¹ · Ludger Schöls^{5,6}

Published online: 15 February 2019

© Springer Science+Business Media, LLC, part of Springer Nature 2019

Abstract

Whole-brain voxel-based morphometry (VBM) studies revealed patterns of patchy atrophy within the cerebellum of Friedreich's ataxia patients, missing clear clinico-anatomic correlations. Studies so far are lacking an appropriate registration to the infratentorial space. To circumvent these limitations, we applied a high-resolution atlas template of the human cerebellum and brainstem (SUIT template) to characterize regional cerebellar atrophy in Friedreich's ataxia (FRDA) on 3-T MRI data. We used a spatially unbiased voxel-based morphometry approach together with T2-based manual segmentation, T2 histogram analysis, and atlas generation of the dentate nuclei in a representative cohort of 18 FRDA patients and matched healthy controls. We demonstrate that the cerebellar volume in FRDA is generally not significantly different from healthy controls but mild lobular atrophy develops beyond normal aging. The medial parts of lobule VI, housing the somatotopic representation of tongue and lips, are the major site of this lobular atrophy, which possibly reflects speech impairment. Extended white matter affection correlates with disease severity across and beyond the cerebellar inflow and outflow tracts. The dentate nucleus, as a major site of cerebellar degeneration, shows a mean volume loss of about 30%. Remarkably, not the atrophy but the T2 signal decrease of the dentate nuclei highly correlates with disease duration and severity.

Keywords Cerebellum · Dentate nucleus · FRDA · MRI · SUIT · VBM · Volumetry

Abbreviations

CSF Cerebrospinal fluid

DN Dentate nucleus

DTI Diffusion tensor imaging

FRDA Friedreich's ataxia

FSL FMRIB software library

FWE Family-wise error

FWHM Full width at half maximum

GAA Guanine-adenine-adenine

GM Gray matter

QSM Quantitative susceptibility mapping

ROI Region of interest

Electronic supplementary material The online version of this article (<https://doi.org/10.1007/s12311-019-1008-z>) contains supplementary material, which is available to authorized users.

✉ Tobias Lindig
tobias.lindig@med.uni-tuebingen.de

¹ Department of Diagnostic and Interventional Neuroradiology, University Hospital Tübingen, Hoppe-Seyler-Str. 3, 72076 Tübingen, Germany

² High-Field MR Center, Max Planck Institute for Biological Cybernetics, Spemannstr. 41, 72076 Tübingen, Germany

³ Department of Psychiatry and Psychotherapy, University Hospital Tübingen, Calwerstr. 14, 72076 Tübingen, Germany

⁴ Institute of Clinical Epidemiology and applied Biometry (IKEaB), University of Tübingen, Silcherstr. 5, 72076 Tübingen, Germany

⁵ Department of Neurology and Hertie Institute for Clinical Brain Research, Eberhard Karls University, Hoppe-Seyler-Str. 3, 72076 Tübingen, Germany

⁶ German Research Center for Neurodegenerative Diseases (DZNE), Otfried-Müller-Str. 23, 72076 Tübingen, Germany

⁷ Department of Biomedical Magnetic Resonance, University Hospital Tübingen, Hoppe-Seyler-Str. 3, 72076 Tübingen, Germany

SARA	Scale for the assessment and rating of ataxia
SD	Standard deviation
SUIT	Spatially unbiased infratentorial template
TFCE	Threshold-free cluster enhancement
TIV	Total intracranial volume
VBM	Voxel-based morphometry
WM	White matter

Introduction

Friedreich's ataxia (FRDA) is the most common autosomal recessive ataxia in the Western world with a frequency of about 1:50,000 individuals. It is clinically characterized by progressive unsteadiness of gait and stance due to predominantly afferent ataxia. The affection of upper limbs and speech develops in later stages of the disease. Cardiomyopathy and diabetes mellitus result from systemic manifestations of FRDA and are seen in about 40% and 7% of patients [1]. Onset is most frequently around puberty but varies between 1 and > 70 years of age [2].

FRDA is caused by lack of frataxin, a mitochondrial protein that is involved in iron-sulfur cluster synthesis which in turn is needed for proper function of the respiratory chain and aconitase. Most patients are homozygous for guanine-adenine-adenine (GAA) repeat expansions in intron1 of the *FXN* gene which lead to impaired transcription [3, 4].

Pathological hallmarks of FRDA [5] include degeneration of sensory neurons in the dorsal root ganglia with consecutive degeneration of dorsal columns of the spinal cord. Additionally, spinal degeneration affects the corticospinal tracts and Clarke's columns with degeneration of the spinocerebellar tracts. In the brain, the dentate nucleus (DN) and the upper cerebellar peduncle are affected. Atrophy of Betz cells and the corticospinal tracts form another intrinsic brain lesion. Cerebellar cortical gray matter is intact in neuropathological studies [5].

Structural MRI of the brain is mostly unremarkable but reveals thinning of the upper cervical cord and mild atrophy of the cerebellum that is often only apparent in later stages of the disease. White matter abnormalities have been found by diffusion tensor imaging (DTI) in the brainstem and upper cerebellar peduncles and the region next to the dentate nucleus [6, 7]. A MR volumetric approach found significant atrophy of the dentate nucleus but no increased iron content in an assessment with 7 T in contrast to earlier reports with 1.5 T [8, 9].

Whole-brain voxel-based morphometry (VBM) studies revealed patterns of patchy atrophy within the Friedreich cerebellum [10–12], missing clear clinico-anatomic correlations. Nonetheless, studies so far are lacking an appropriate registration to the infratentorial space, since the commonly used standard atlas template (MNI whole-brain template ICBM152)

provides very little contrast for cerebellar structures and is thus prone to misregistration and artifacts.

To circumvent these limitations and to develop clinically meaningful imaging biomarkers in FRDA, we applied a high-resolution atlas template of the human cerebellum and brainstem (SUIT template, Brain and Mind Institute 2017) to characterize regional cerebellar atrophy in Friedreich's ataxia. We used a spatially unbiased voxel-based morphometry approach together with T2-based manual segmentation and T2 histogram analysis and obtained probabilistic maps of the dentate nuclei in a representative cohort of FRDA patients. To investigate the influence of disease duration and disease severity on imaging findings, we correlated gray and white matter concentrations, cerebellar volumes, and dentate volume and dentate T2 values with clinical data.

Materials and Methods

Subjects and Study Design

The prospective cross-sectional study was approved by the local ethics review board. Informed written consent was obtained from all subjects prior to examinations. Subjects were enrolled after screening for inclusion and exclusion criteria over a period of 29 months. Inclusion criteria were a genetic diagnosis of FRDA, age over 18 years, no other neurological or psychiatric disease, no major medical comorbidity or substance abuse that could interfere with cognitive function, and no other alterations at routine MR imaging of the brain. Exclusion criteria were common contraindications for MR imaging. Healthy controls were included only if they had normal findings in the medical history assessment, neurological examination, and on routine MRI. Twenty adult patients with confirmed GAA repeat expansions in intron1 of the *FXN* gene (mean age 34.9 ± 14.2 ; 6 females, 14 males; all right-handed) and 20 plus 3 age- and sex-matched healthy controls (mean age 35.9 ± 13.9 ; 6 females, 14 males; all right-handed) were recruited from the ataxia outpatient clinic in Tübingen and by word of mouth. Three additional controls had to be recruited to compensate for the drop out of three subjects due to movement artifacts [2] and one normalization failure [1] during data preprocessing of additional acquired DTI data not included in this study. A total of four different methods were applied in this study; therefore, detailed demographics and clinical characteristics of all patients and controls for each separate analysis are provided in Table 1. All subjects underwent full medical history and neurological examination including the scale for the assessment and rating of ataxia (SARA) as a validated measure of disease severity [13, 14]. Six FRDA patients analyzed had late onset of the disease.

Table 1 Demographics and clinical characteristics of FRDA patients and controls

	SUIT-VBM/volumetric analysis			Dentate T2-based analysis		
	FRDA patients (<i>n</i> = 15; 18), mean (SD)	Controls (<i>n</i> = 15; 22), mean (SD)	<i>p</i> value	FRDA patients (<i>n</i> = 13), mean (SD)	Controls (<i>n</i> = 21) mean (SD)	<i>p</i> value
Demographics						
Age (years)	31.7/34.9 (11.5/14.2)	32.9/35 (11.5/13.5)	.77/.98	35.5 (15.8)	34.5 (13.6)	.85
Gender (female; male)	5; 6/10; 12	5; 6/10; 16		3/10	6/15	
Handedness (right; left)	15; 0/18; 0	15; 0/22; 0		13/0	21/0	
Clinical measures						
Age of onset (years)	19.2/19.9 (8.9/10)	n.a.		22.9 (10.8)	n.a.	
Disease duration (years)	12.5/14.9 (5.8/8)	n.a.		12.7 (7.4)	n.a.	
SARA total score	16.9/18.9 (7.1/8.7)	n.a.		14.5 (6.3)	n.a.	

SD standard deviation, FRDA Friedreich's ataxia, SARA scale for the assessment and rating of ataxia, n.a. not applicable

MR Imaging Data Acquisition

MRI was performed on a 3-T whole-body MR system (MAGNETOM Trio Tim, Siemens, Erlangen, Germany) using a 32-channel head coil. Diagnostic MRI was carried out to exclude pathological conditions not related to FRDA such as tumor, infarction, or other focal lesions. Structural 3D volume data were collected with T1 contrast and T2 contrast: MPRAGE (TR/TE/TI, 2300/3.51/900 ms; voxel size, 1 mm isotropic; acquisition time, 6.75 min) and 3D T2 TSE (TR/TE, 3200/307 ms; voxel size, 0.7 mm isotropic; acquisition time, 13.5 min).

Infratentorial VBM (Gray Matter/White Matter)

Voxel-based morphometry of infratentorial structures was carried out on T1-weighted images using the spatially unbiased infratentorial template of the SUIT toolbox (Version 2.7, Brain and Mind Institute 2017) [15, 16]. From the 20 datasets of FRDA patients, one scan had to be excluded due to movement artifacts, and one scan due to an incidental finding (infratentorial vascular malformation).

After a linear normalization step, the cerebellum and brainstem were segmented into tissue types using the statistical parametric mapping (SPM)12 segmentation algorithm (Wellcome Trust Centre 2017) [17, 18], isolated from the surrounding non-brain and supratentorial brain structures, and cropped to an infratentorial volume of interest. All isolation maps were hand-corrected to exclude tissue of the occipital lobe and venous sinuses using MRICron, a 3D image viewer by Chris Rorden (Chris Rorden's Neuropsychology Lab 2017) [19]. The cropped images were then normalized to a spatially unbiased atlas template of the cerebellum and brainstem. The segmented gray and white matter images were re-sliced into SUIT space using the deformation map generated in the normalization step.

The resulting infratentorial segmentation maps of normal controls and FRDA patients were then checked for group homogeneity using the VBM toolbox VBM8 to calculate the standard deviation across the sample (Structural Brain Mapping Group 2017). Three patients and one control with a covariance of and below two standard deviations were identified as outliers and consequently excluded from further VBM analysis together with their healthy matched controls. The conspicuous control was replaced by another matched control. This resulted in 15 patients and their matched controls being analyzed (Table 1).

The segmented normalized and modulated infratentorial images were then smoothed by a $6 \times 6 \times 6$ -mm full width at half maximum (FWHM; sigma 3) Gaussian smoothing kernel. Differences between the two groups were analyzed by voxel-wise cross-subject statistics using a permutation-based inference tool for nonparametric statistical thresholding with 5000 permutations. Age, sex, and total intracranial volume (TIV) were used as covariates to perform nonparametric permutation inference by carrying out TFCE (threshold-free cluster enhancement) [20, 21]. The mean centering of age and TIV was performed for the patient and the control group. Mean-centered values were computed by subtracting subject-specific values one by one from the group mean (Center for Investigating Healthy Minds 2017). The permutation inference using TFCE was computed using the randomise tool from FMRIB software library (FSL) (FMRIB 2017) [22]. An absolute threshold masking of 0.2 was used to restrict the analysis to gray and white matter, respectively. TFCE family-wise error corrected $p \leq 0.05$ was considered the level of significance. Flatmaps were visualized using SUIT toolbox's MATLAB scripts [23].

Voxel-wise statistically significant relationships of cerebellar gray matter (GM) and white matter (WM) volumes with the regressors age, sex, TIV, disease duration, and SARA total score were calculated for the group of FRDA patients by

voxel-wise cross-subject statistics using FSL randomise. Nonparametric permutation inference ($N = 5000$) was calculated by carrying out TFCE as described for the group analysis above. TFCE family-wise error corrected $p \leq 0.05$ was considered the level of significance if not stated otherwise.

Cerebellar Volumetry

The individual volume of the cerebellum was calculated in analogy to Ridgway and Malone [24, 25] as a combination of the modulated nonlinearly warped GM and WM cerebellar volumes from the SUI pipeline. The segmented normalized and modulated infratentorial GM and WM volumes (with wcm prefixes) were masked with a whole cerebellar label map in SUI space and finally added. GM and WM cerebellar volumes were calculated, respectively. With regard to individual volumetry, the three previously (in the VBM group analysis) excluded patients with a covariance below two standard deviations across the sample could be included after careful visual inspection to ensure image quality and exclude artifacts in the image. The previously excluded control remained excluded due to poor normalization to the cerebellar template. This resulted in 18 patients and 22 controls being analyzed (Table 1).

We calculated cerebellar volumes as the fraction of total intracranial volume (TIV) to evaluate atrophy independent of head size. TIV was calculated from T1-weighted images as the sum of the modulated nonlinearly warped GM, WM, and cerebrospinal fluid (CSF) whole-brain volumes using SPM12 segmentation [25]. To evaluate differences in cerebellar volumes of patients and controls, unpaired t tests were used. The Pearson correlation coefficients were calculated for age, disease duration, and SARA score using IBM SPSS 23.0.0 statistical software and were corrected for multiple comparisons (Bonferroni-Holms). The level of significance was set to $p \leq 0.05$. Cerebellar volumes with subfractions (GM, GM minus lobule VI, WM, and CSF) were plotted against age.

Dentate Volumetry

The DN is not delineated on T1-weighted images and thus cannot be evaluated by standard T1-based VBM procedures. Instead, the volumes of the DN were manually segmented on 3D high-resolution T2 images by an experienced and blinded neuroradiologist using ITK-SNAP software (version 3.4, Penn Image Computing and Science Laboratory, and Scientific Computing and Imaging Institute 2017) [26]. Due to magnetic susceptibility effects and a short T2 time caused by high iron content, the DN appear hypointense on T2-weighted images compared to the surrounding tissue (Fig. 4a). Five patients and one control had to be excluded because of lack of T2 high-resolution volume data. Another

two patients and one control had to be discarded after visual inspection due to insufficient imaging quality of the data with poor delineation of the DN. This resulted in 13 patients and 21 controls being analyzed (Table 1).

Probabilistic maps of left and right DN were calculated for the patient ($n = 13$) and the control ($n = 21$) group. Therefore, whole-brain structural T1 scans were oriented to the anterior commissure as the origin (0, 0, 0). The manually drawn (ITK-SNAP) dentate region of interest (ROI) was affine-transformed into oriented T1 image space. The T1 images were segmented and the cerebellum was isolated from each T1 using SUI toolbox [16]. The dentate-specific normalization method implemented in SPM-SUI toolbox [27] was used to register T1 space dentate ROI into SUI space. The registered dentate ROIs were then summed up and divided by the number of all patients or controls to create the probabilistic maps, respectively. A dentate fixed effect group analysis was performed on the averaged dentate ROIs of all patients and controls.

We calculated DN volumes as the fraction of total intracranial volume (TIV) to evaluate atrophy independent of head size. TIV was calculated from T1-weighted images as the sum of the modulated nonlinearly warped GM, WM, and CSF whole-brain volumes using SPM12 segmentation [25]. To evaluate differences in DN volumes of patients and controls, unpaired t tests were used. The Pearson correlation coefficients were calculated for age, disease duration, and SARA score using IBM SPSS 23.0.0 statistical software and were corrected for multiple comparisons (Bonferroni-Holms). The level of significance was set to $p \leq 0.05$.

Dentate T2 Signal Analysis

Furthermore, dentate T2 signal intensity histograms of FRDA and control group were calculated. Therefore, voxel-based T2 values of all dentate volumes were plotted as kernel density estimate for bivariate distribution and evaluated using an unpaired two-sample t test. T2 signal intensity was adjusted by dividing the signal intensity of each dentate voxel with the mean intensity of the CSF of the fourth ventricle.

Results

Infratentorial VBM (Gray Matter/White Matter)

Voxel-based analysis of cerebellar gray matter ($p < 0.05$ TFCE family-wise error (FWE) corrected) with SUI revealed bilateral volume reduction in the medial parts of lobule VI in FRDA patients and to a lesser extent in the neighboring right crus I and II of the posterior cerebellar lobe (Fig. 1). By lowering the p value to $p < 0.1$ TFCE FWE corrected, the left crus

I and II also showed a bilateral symmetric volume reduction, reflecting low statistical power for this small effect.

Voxel-wise comparison of the infratentorial white matter ($p < 0.05$ TFCE FWE corrected) between FRDA patients and controls (Fig. 2) demonstrated bilateral affection of the cerebellar inflow and outflow tracts with volume reduction of the inferior and superior cerebellar peduncles, respectively. Additionally, for the apical peri-dentate white matter, especially between dentate and lobule VI, respectively, the superior cerebellar peduncles were atrophic. In line with the affected in- and outflow tracts, the inferior medulla and the decussation of the superior cerebellar peduncles showed white matter atrophy.

As expected, there was no significant increase in gray or white matter concentration in patients compared to controls.

In the group of FRDA patients, regression analysis (Figs. 1 and 2) (adjusted for age, sex, and TIV) revealed significant negative correlations between white matter concentration and SARA score for the dorso-apical peri-dentate cerebellar white matter, the inferior, middle and superior cerebellar peduncles, and major parts of the brainstem including the pons and midbrain. Significant negative correlations between gray matter and SARA score could only be shown for medial parts of left crus I and to a lesser extent also for the adjacent crus II. Corresponding parts on the right hemisphere were regressed out by a significant negative correlation with age. Thus, by lowering the p value to $p < 0.1$ TFCE FWE corrected, the bilateral symmetric relation with SARA score could also be shown for right crus I and II. For disease duration, significant negative correlations could be shown in the lateral white matter of the pons and midbrain predominantly on the right side. No correlation with disease duration could be shown for gray matter concentration.

Cerebellar Volumetry

Significant negative correlation coefficients could be shown in FRDA patients but not in controls for cerebellar gray matter volume (fraction of TIV) and age (FRDA $r = -.62$, $p = .006$; and controls $r = -.28$, $p = .21$), although no significant volume difference for total cerebellar volume could be found after correction for TIV over all patients and subjects. Global cerebellar volumes of FRDA patients (fraction of TIV) plotted against age suggest a mild cerebellar atrophy in later stages of the disease (Fig. 3a) in accordance with well-established impressions from routine MRI, but miss significance for the total cerebellar volume. Interestingly, FRDA cerebellum aged 18 to 40 years shows no difference from healthy controls (Fig. 3b). Furthermore, the suggested global atrophy in later stages of the disease seems to be attributed to a predominant atrophy of the gray matter, which is not restricted to lobule VI alone (Fig. 3c), as suggested from the VBM results above. Thus, the steepness of the correlation lines in Fig. 3c nearly stays the

same for both conditions of cerebellar gray matter (fraction of TIV) with and without lobule VI (with: $y = 0.0689 - 0.0003 \times x$; without $y = 0.0568 - 0.0003 \times x$). Significant correlations with disease duration could be shown for patient total cerebellar volume ($r = -.71$; $p < .001$) and gray matter volume ($r = -.77$; $p < .001$) and with SARA score for patient total cerebellar volume ($r = -.69$; $p = .002$), gray matter volume ($r = -.52$; $p = .03$), and white matter volume ($r = -.72$; $p < .001$), all as fraction of TIV.

Dentate Volumetry

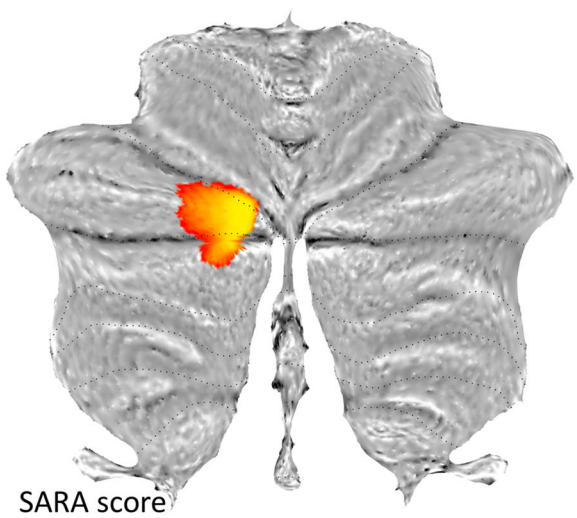
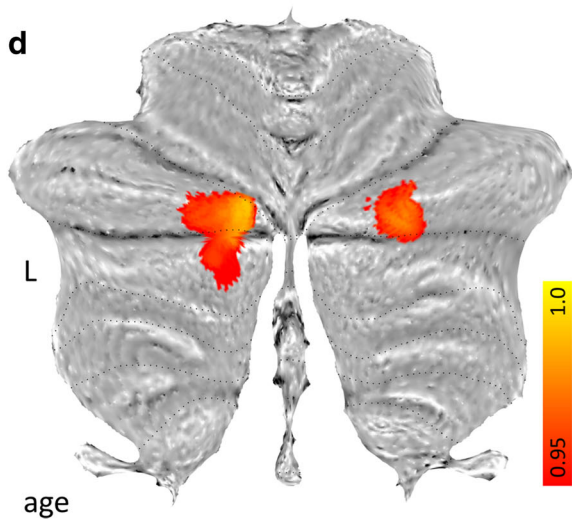
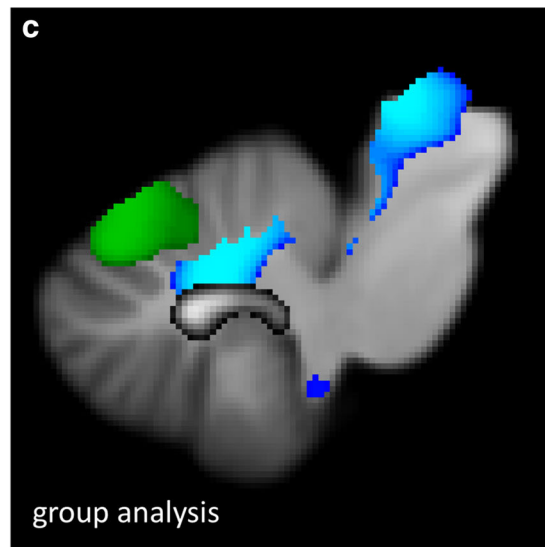
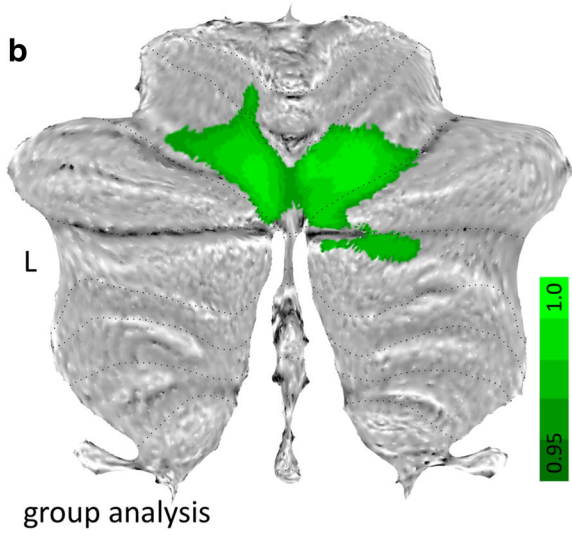
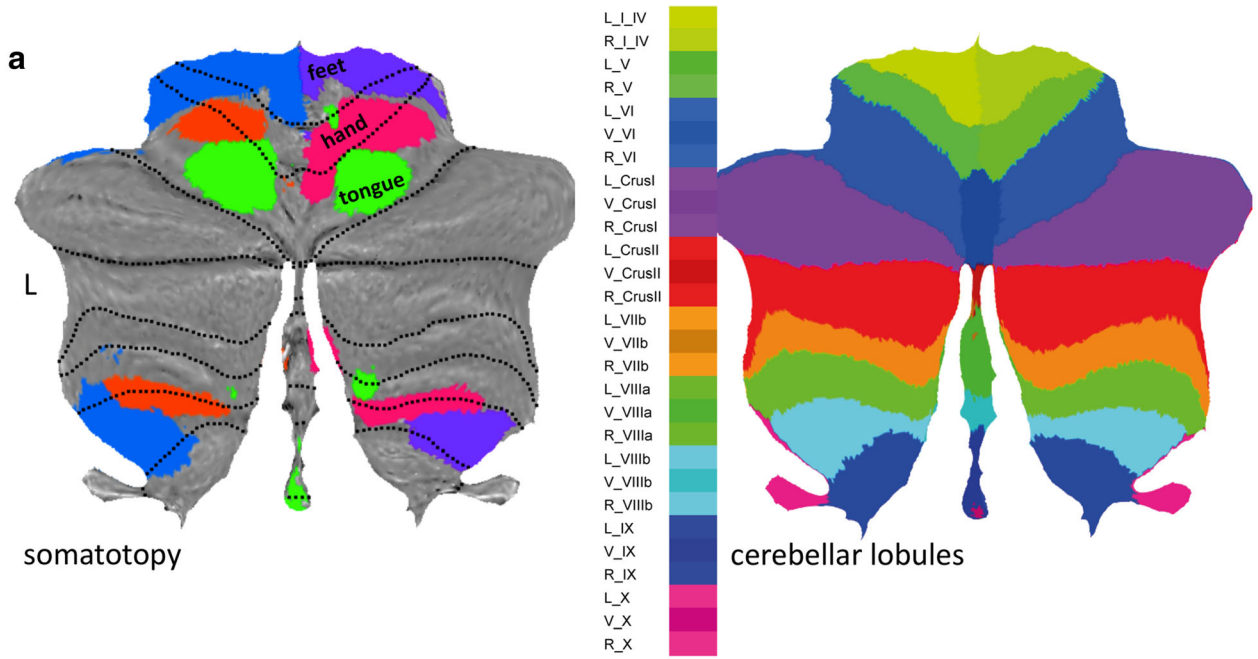
Dentate atrophy in FRDA patients [5, 8] could be confirmed on high-resolution T2-weighted images with a clinical 3-T Scanner (Fig. 4). Volume of the DN (fraction of TIV) was significantly smaller in FRDA patients compared to controls ($p < .001$; mean absolute volume of bilateral nuclei in FRDA 1.65 ml, SD 0.41; and controls 2.43 ml, SD 0.37), although DN volume could not be determined in two patients and one control, due to insufficient low visibility of the nuclei for correct assessment. No significant correlations could be shown for the DN volume with age ($r = .07$; $p = .83$), disease duration ($r = .09$; $p = .77$), and SARA score ($r = .33$; $p = .27$). Fixed effects group analysis on the dentate (Fig. 4c) and visual inspection of the probabilistic atlases of DN from patients and controls in 3D demonstrated a generalized shrinking of the DN in FRDA with relative sparing of the dorsal parts and most prominent atrophy in the ventro-rostral and medial parts. In FRDA patients, the lateral parts of the dentate appeared more T2 hypointense compared to controls.

Dentate T2 Signal Analysis

T2 signal intensity histogram analysis (Fig. 4d) revealed significantly lower relative T2 signal intensities of the dentate tissue in FRDA patients compared to controls ($T = 46.18$; $p < .001$). Patients' T2 mean values correlated significantly with disease duration ($r = -.84$; $p < .001$) and SARA score ($r = -.76$; $p = .003$), but not with age ($r = -.47$; $p = .10$) nor with dentate volume ($r = -.20$; $p = .52$).

Discussion

Our results demonstrate a substantial cerebellar atrophy, which beyond the in- and outflow tracts and the dentate nucleus predominantly affects the medial parts of lobule VI, the somatotopic representation of tongue and lips. Remarkably, with regard to the dentate nucleus as the major site of cerebellar degeneration, it is not the considerable atrophy but the T2 signal decrease which highly correlates with disease duration and severity.



◀ **Fig. 1** SUI-VBM results for cerebellar gray matter. **a** On the left, somatotopic cerebellar representations for hand (left red; right pink), foot (left blue; right purple), and tongue (green) movements are displayed on a cerebellar flatmap; adapted from Diedrichsen J and E Zotow 2015, original Fig. 7A [21]. On the right, anatomical locations of the different cerebellar lobules are shown on the cerebellar flatmap for orientation. **b** Gray matter VBM group results (FRDA < controls) are displayed as cerebellar flatmap; significant atrophy in FRDA patients is displayed in green. **c** The gray matter VBM group results (FRDA < controls) together with the corresponding white matter results demonstrate the close neuroanatomical relationship of the atrophic lobule VI (green) and the dentate nucleus (gray) with atrophied white matter (blue) in between the two structures; depicted in sagittal plane on the SUI template. **d** Significant relationships between gray matter concentration and age (left)/SARA score (right) are shown as cerebellar flatmap

Infratentorial VBM (Gray Matter/White Matter)

Imaging cerebellar affection in FRDA with a registration technology optimized for the infratentorial space revealed detailed affection of cerebellar gray and white matter, which correlates well with clinical deficits in patients. Atrophy of the inferior cerebellar peduncle matches nicely impaired afferent input from the spinocerebellar tracts that are severely degenerated in FRDA and leads to afferent ataxia, a hallmark of FRDA.

As the dentate nucleus forms the major outflow tracts of the cerebellum, leaving the cerebellum through the superior

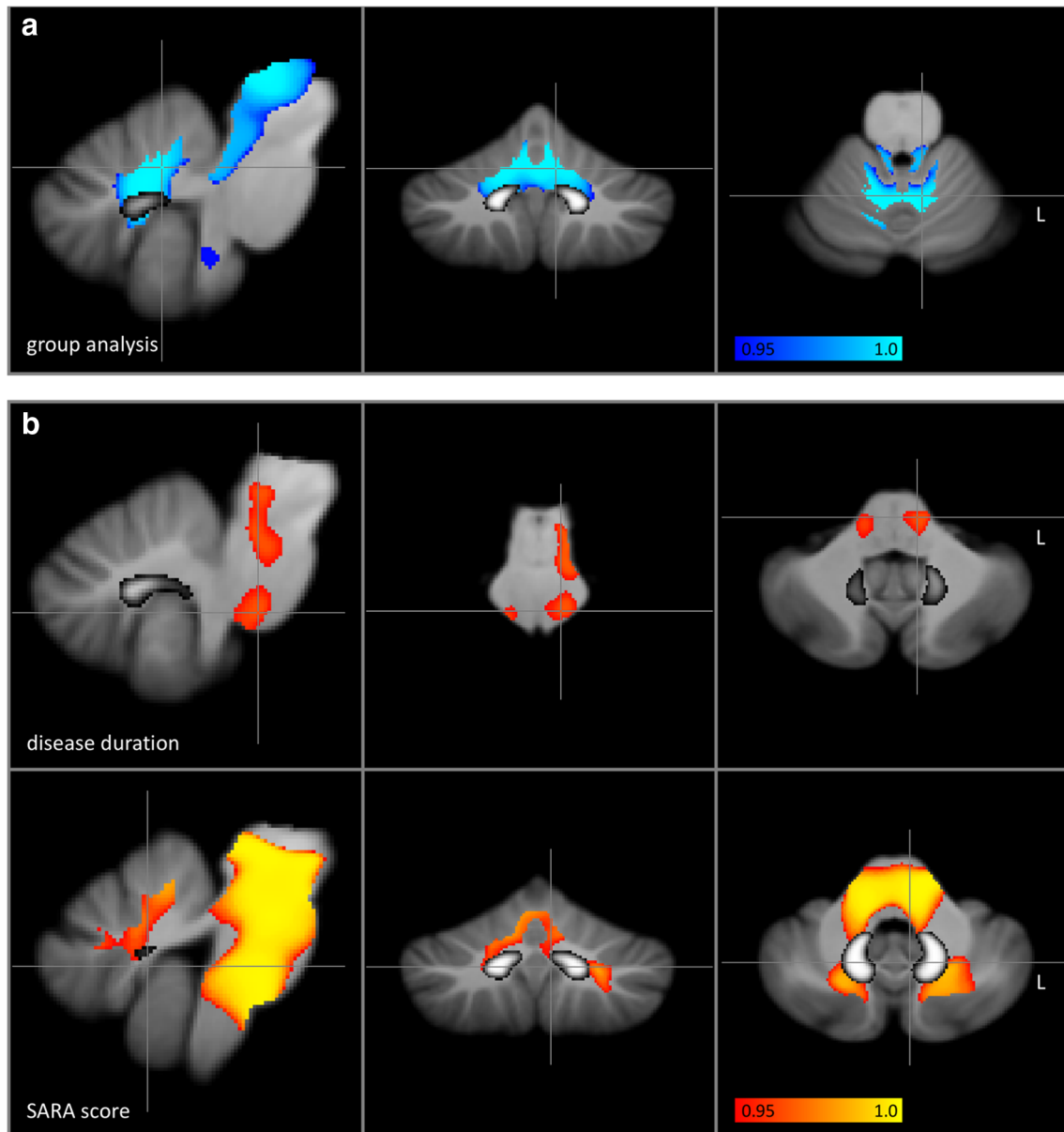
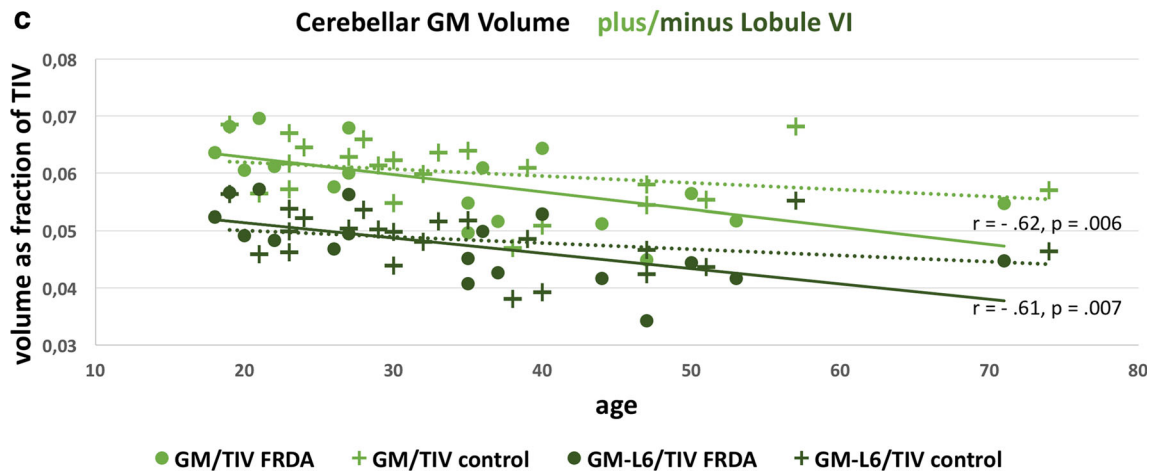
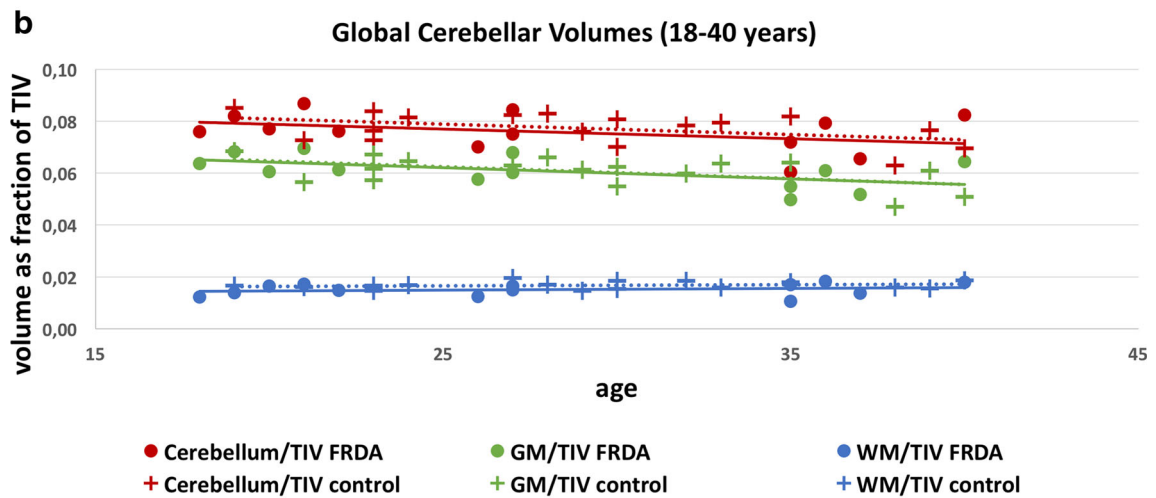
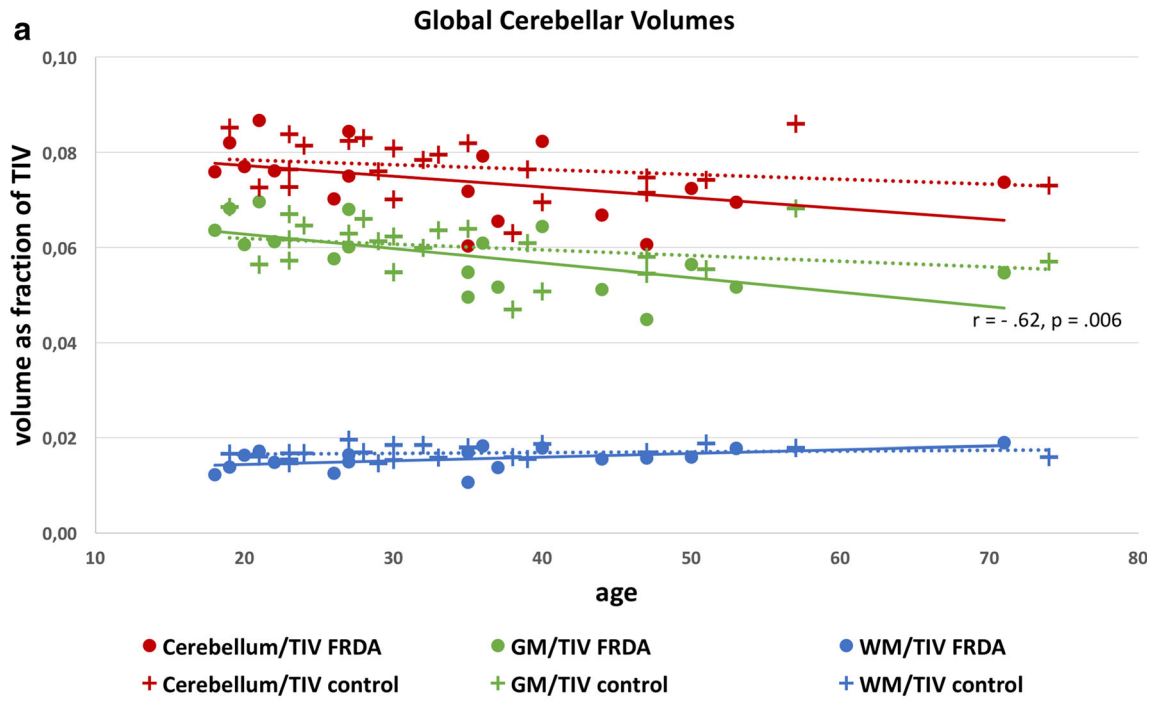


Fig. 2 SUI-VBM results for cerebellar white matter. **a** White matter VBM group results (FRDA < controls) are depicted in sagittal, coronal, and axial plane on the SUI template; significant atrophy in FRDA patients is displayed in blue. **b** Significant relationships (red) between

white matter concentration and disease duration (upper row)/SARA score (lower row) are shown in sagittal, coronal, and axial plane on the SUI template. FRDA dentate group fixed effects map (gray) demonstrates the anatomical relation to the dentate nucleus



◀ **Fig. 3** Atlas-based volumetry of the cerebellum. **a** Global cerebellar volumes (total, gray matter, and white matter) as fraction of TIV are plotted against age for FRDA patients and healthy controls. Correlation lines are included for FRDA: total $r = -.42$, $p = .08$, gray matter $r = -.62$, $p = .006$, and white matter $r = -.48$, $p = .04$; and controls: total $r = -.23$, $p = .30$, gray matter $r = -.29$, $p = .21$, and white matter $r = .17$, $p = .48$. In **b**, only the age range of early adulthood from 18 to 40 years is shown. Correlation lines are included for FRDA: total $r = -.38$, $p = .20$, gray matter $r = -.55$, $p = .05$, and white matter $r = -.23$, $p = .46$; and controls: total $r = -.43$, $p = .08$, gray matter $r = -.51$, $p = .04$, and white matter $r = .20$, $p = .44$. **c** Cerebellar gray matter volumes (total gray matter and gray matter with exclusion of lobule VI) as fraction of TIV are plotted against age in FRDA and controls. Correlation lines are displayed for FRDA: total gray matter $r = -.62$, $p = .006$, gray matter with exclusion of lobule VI $r = -.61$, $p = .007$; and controls: total gray matter $r = -.29$, $p = .21$, gray matter with exclusion of lobule VI $r = -.30$, $p = .18$

peduncle, our finding of atrophy in the upper cerebellar peduncle nicely mirrors this functional and anatomical connection. The extended affection of the WM beyond the cerebellar inflow and outflow tracts with close relation to disease severity gives hint for further evaluations of the brainstem using DTI biomarkers, with the urgent need for applying distinct registration algorithms to account for the variability of the infratentorial space, which is not included in most widely used standard brain registration procedures.

Functional MRI studies in FRDA could recently show alterations of functional MR signals in the cerebellar cortex [28–33] indicating neurodegenerative processes beyond the dentate nucleus. In line with this and in addition to a very slow and general atrophy of the cerebellar gray matter beyond normal aging, our study demonstrates that FRDA patients develop a predominant bilateral atrophy in the medial parts of lobule VI. This part of the cerebellum is known to be crucially engaged in the control of sequences of articulatory movements and also of non-speech oral motor movements, a fact that is based on the results of many functional imaging studies providing markedly consistent results with regard to the mentioned role of lobule VI. On the one hand, it was demonstrated that a bilateral somatotopy of the lips and tongue can be located in lobule VI [23, 34, 35]. On the other hand, a series of functional imaging studies reported robust hemodynamic responses in lobule VI associated with various speech motor and non-speech oral motor tasks [36]. Against this background, it should be mentioned that almost all patients with FRDA will develop speech impairments [37, 38] which can be described as rather mild even after a longer disease duration [39, 40]. However, the severity of dysarthria was reported to be unrelated with the severity of ataxia [39]. This might be in turn one reason why in the present study, no correlation could be shown between the atrophy of lobule VI and the SARA score in which the rating of speech is only a minor aspect. The hypothesized relationship between the significant atrophy of lobule VI which is

not so pronounced that it is obviously visible by routine MRI, and the rather mild severity of speech motor disorder observed in FRDA, needs to be further investigated in longitudinal studies and larger patient cohorts.

Cerebellar Volumetry

There is a long-lasting debate as to whether the cerebellum in FRDA appears normal in clinical imaging or not. In our study limited to 18 patients, we could only show a mild cerebellar atrophy in later stages of the disease, which was distinct from normal aging. More importantly, in the age range of early adulthood from 18 to 40 years, no differences of cerebellar volume could be detected between FRDA patients and healthy controls. Our findings underpin the clinical impression that the cerebellum looks normal in Friedreich's ataxia [37, 41]. Thus, a radiologically normal appearing cerebellum of a younger patient with ataxia supports the diagnosis of FRDA and decreases the likelihood of other less frequent recessive [42] or autosomal dominant [43] ataxias, which may have cerebellar atrophy. In older patients, it will be difficult to distinguish cerebellar atrophy from normal aging because it has only a minor degree of cerebellar atrophy.

Dentate Volumetry

The dentate nucleus is well established by pathoanatomical studies as the major site of cerebellar degeneration in FRDA [44]. Using high-resolution T2 volume datasets of 0.343 mm^3 isotropic voxel size, we could quantify dentate atrophy with a volume loss of about 30% compared to controls. As the dentate nucleus forms the dominant outflow tract of the cerebellum, this rather focal affection can explain the strong effect on ataxia of gait and limbs despite otherwise rather well-preserved cerebellar structures. Interestingly, volumetry did not prove correlations of degeneration of the dentate nucleus with disease severity or age, indicating that the degenerative process at the dentate nucleus may occur rather early in the disease process and thus may be neurodevelopmental. Alternatively, the small volume changes (0.8 ml in total) may escape further graduation for correlation analyses. This may be revealed in longitudinal studies when volumetric data become available from follow-up assessments for individual patients.

Additionally, fixed effects group analysis revealed in FRDA patients, besides a generalized shrinking of the dentate nucleus with relative sparing of the dorsal parts, the most prominent atrophy in the ventro-rostral and medial parts. The latter corresponds nicely to the origin of the superior cerebellar peduncle, where the efferent fibers of the degenerating large glutamatergic neurons of the

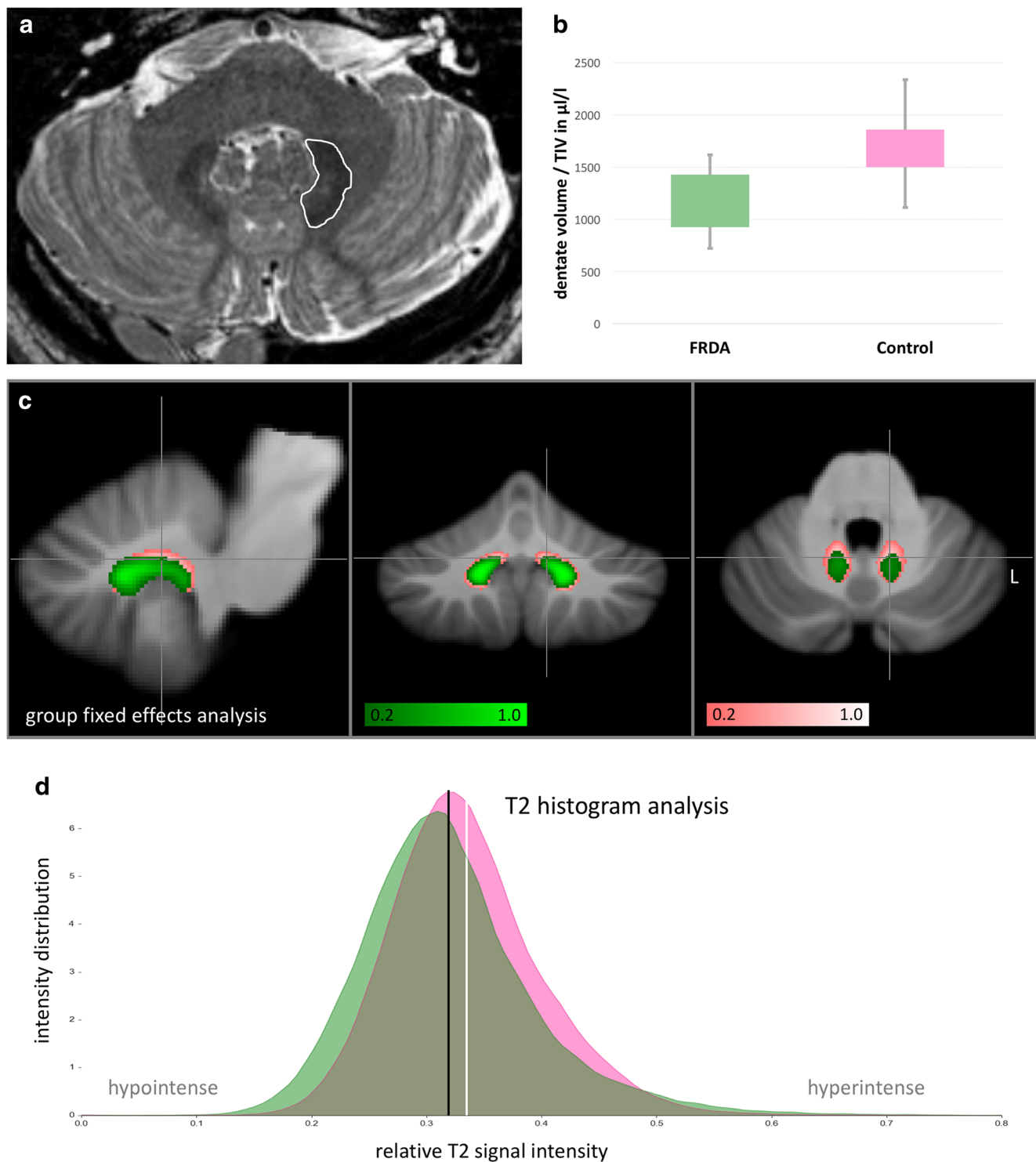


Fig. 4 Volumetry and T2 histogram analysis of the dentate nuclei. **a** Typical depiction of the dentate nucleus on a high-resolution axial T2 image of a patient with Friedreich's ataxia used for manual segmentation (white segmentation line). **b** Volumes of the dentate nucleus as a fraction of TIV in FRDA vs. controls are displayed as boxplot. **c** Dentate group fixed effects analysis shown in sagittal,

coronal, and axial views with FRDA in green vs. controls in pink, thresholded for 0.2. **d** Dentate T2 signal intensity histograms of FRDA (green) and control group (pink): adjusted voxel-based T2 values of all dentate volumes are plotted as kernel density estimate for bivariate distribution; FRDA mean—black vertical line, control mean—white vertical line

dentate reside [45]. Since already in healthy subjects, the iron content of the dorsal parts of the dentate is less than

of the ventral parts, MRI imaging of the dentate nucleus in FRDA is prone to miss this part.

Dentate T2 Signal Analysis

T2 signal intensity histogram analysis of the dentate nucleus confirmed a significant reduction in T2 relaxation time in FRDA patients compared to controls [9, 46, 47], in line with an ongoing debate as to whether this is mainly due to iron accumulation or to atrophy. Our study adds to the discussion the fact that the observed atrophy of the dentate nucleus is not correlated to the signal decrease and thus, tissue atrophy is most likely not the source of the signal decrease. Furthermore, the observed T2 signal decrease highly correlates with disease duration and severity (SARA score) but not with age, given together with another recent study [47] accumulating evidence that T2 relaxometry could serve as a reliable biomarker. Remarkably, we could show this relation can already be observed on standard T2-weighted imaging and without applying more difficult procedures like the T2 mapping demonstrated by Bonilha da Silva et al. [47]. The iron accumulation hypothesis, which was not the focus of our study, is still ambiguous since histopathologic [48] and ultra-high field studies [8, 48, 49] revealed no iron accumulation. On the other hand, a recent quantitative susceptibility mapping (QSM) study on 35 FRDA patients [50] demonstrated elevated iron concentration in the extrapyramidal motor system in FRDA including the DN. Since QSM is a robust technique for any quantification of para-/ferromagnetic substances, this is a strong hint for iron dyshomeostasis within the dentate nucleus. On the other hand, changes in local tissue microstructure can also affect both T2 relaxation and phase evolution (as the basis of QSM imaging) and might therefore explain the altered T2 contrast.

Limitation and Strength of the Study

Limitations of the study are, besides the abovementioned cross-sectional design and the limited sample size, the inclusion of patients with late-onset FRDA, who vary in clinical disease progression and severity from individuals with typical FRDA. Therefore, larger samples of subgroups are needed. Small sample sizes are an inherent issue working with rare diseases, a drawback that has to be overcome by accumulating more evidence through an emerging number of clinical studies and pooling of data from different sites, recently introduced by the ENIGMA-Ataxia neuroimaging working group <http://enigma.ini.usc.edu/ongoing/enigma-ataxia/>. Another limitation of our study results from the fact that there is a close spatial relationship between the atrophic lobules VI and the dentate nucleus with atrophic white matter between these two structures. While probabilistic maps of the white matter tracts [51] in this region suggest that both

afferent and efferent fiber tracts are probably affected, the direct link between lobules VI and the dentate nucleus with fiber tracking is missing in our volumetric study.

The strength of the study is the combined approach of an exploratory VBM analysis focused on the infratentorial SUIT space in conjunction with a manual and semiautomatic atlas-based volumetry of the individual space. In the research on FRDA, this is, to our knowledge, the first study to apply the spatially unbiased SUIT framework with the improved inter-individual alignment of cerebellar structures. The SUIT template preserves the anatomical details of the cerebellum and reduces spatial variance to a third compared to current evaluation methods using the MNI whole-brain template (Brain and Mind Institute 2017). To avoid the recently emerging problems [52, 53] of standard family-wise error correction using false discovery rate (FDR), we applied a threshold-free cluster enhancement (TFCE) instead, a permutation-based inference tool for nonparametric statistical thresholding. Considering our small sample size, we tried to improve the homogeneity and quality of our cohort. MRI datasets were carefully and conservatively checked for any imaging artifacts like movement, and pathologies not related to FRDA were excluded from further analysis. The standard deviation across the sample was calculated to assure group homogeneity (see Structural Brain Mapping Group 2017).

Conclusion

With a detailed focus on the infratentorial space, we could provide further insight into the close anatomical relationship of cerebellar gray and white matter affection in Friedreich's ataxia beyond the well-known atrophy of the dentate nucleus (see [supplementary video material](#)). We have demonstrated that FRDA patients not only develop cerebellar atrophy that is minor in degree but distinct from normal aging, but also evolve a predominant lobular atrophy of the medial parts of lobule VI, containing the somatotopic representation of tongue and lips. We show a close spatial relationship between the atrophic lobule VI and the dentate nucleus with atrophied white matter in between the two structures. Furthermore, we here demonstrate that the dentate T2 signal decay determined from standard T2 TSE sequences could serve as a clinically suitable biomarker correlating with the duration and the severity of the disease, whereas the atrophy of the DN correlates neither with the T2 signal nor with the duration and severity of the disease. Our study not only provides detailed evidence of GM affection beyond the dentate, but also emphasizes the need for further studies for example to establish reliable DTI biomarkers to assess WM tract affections in relation with disease severity across and beyond the dentate outflow tracts.

Acknowledgments The authors wish to thank Merim Bilalic and Matthew Bladen for proof-reading of the manuscript and language editing.

Funding This work was supported by the European Union by a grant to EFACTS (HEALTH-F2-2010-242193) and the Else-Kröner Fresenius Stiftung (to MS).

Data Availability The dentate atlases of FRDA patients and normal controls will be made available by the authors on request. Requests can be made via e-mail to either Tobias Lindig (Tobias.Lindig@med.uni-tuebingen.de) or Benjamin Bender (Benjamin.Bender@med.uni-tuebingen.de).

Compliance with Ethical Standards

Conflict of Interest The authors declare that they have no conflict of interest.

Ethical Approval All procedures performed in studies involving human participants were in accordance with the ethical standards of the institutional and/or national research committee and with the 1964 Helsinki declaration and its later amendments or comparable ethical standards. Informed consent was obtained from all individual participants included in the study. This article does not contain any studies with animals performed by any of the authors.

Publisher's Note Springer Nature remains neutral with regard to jurisdictional claims in published maps and institutional affiliations.

References

- Reetz K, Dogan I, Hohenfeld C, Didszun C, Giunti P, Mariotti C, et al. Nonataxia symptoms in Friedreich ataxia: report from the registry of the European Friedreich's Ataxia Consortium for Translational Studies (EFACTS). *Neurology*. 2018;91(10):e917–e30.
- Reetz K, Dogan I, Costa AS, Dafotakis M, Fedosov K, Giunti P, et al. Biological and clinical characteristics of the European Friedreich's Ataxia Consortium for Translational Studies (EFACTS) cohort: a cross-sectional analysis of baseline data. *Lancet Neurol*. 2015;14(2):174–82.
- Schmucker S, Puccio H. Understanding the molecular mechanisms of Friedreich's ataxia to develop therapeutic approaches. *Hum Mol Genet*. 2010;19(R1):R103–10.
- Pastore A, Puccio H. Frataxin: a protein in search for a function. *J Neurochem*. 2013;126(Suppl 1):43–52.
- Koepfen AH, Mazurkiewicz JE. Friedreich ataxia: neuropathology revised. *J Neuropathol Exp Neurol*. 2013;72(2):78–90.
- Pagani E, Ginestroni A, Della Nave R, Agosta F, Salvi F, De Michele G, et al. Assessment of brain white matter fiber bundle atrophy in patients with Friedreich ataxia. *Radiology*. 2010;255(3):882–9.
- Della Nave R, Ginestroni A, Tessa C, Salvatore E, Bartolomei I, Salvi F, et al. Brain white matter tracts degeneration in Friedreich ataxia. An in vivo MRI study using tract-based spatial statistics and voxel-based morphometry. *NeuroImage*. 2008;40(1):19–25.
- Solbach K, Kraff O, Minnerop M, Beck A, Schols L, Gizewski ER, et al. Cerebellar pathology in Friedreich's ataxia: atrophied dentate nuclei with normal iron content. *Neuroimage Clin*. 2014;6:93–9.
- Waldvogel D, van Gelderen P, Hallett M. Increased iron in the dentate nucleus of patients with Friedreich's ataxia. *Ann Neurol*. 1999;46(1):123–5.
- Rezende TJ, Silva CB, Yassuda CL, Campos BM, D'Abreu A, Cendes F, et al. Longitudinal magnetic resonance imaging study shows progressive pyramidal and callosal damage in Friedreich's ataxia. *Mov Disord*. 2016;31(1):70–8.
- Selvadurai LP, Harding IH, Corben LA, Stagnitti MR, Storey E, Egan GF, et al. Cerebral and cerebellar grey matter atrophy in Friedreich ataxia: the IMAGE-FRDA study. *J Neurol*. 2016;263:2215–23.
- Della Nave R, Ginestroni A, Giannelli M, Tessa C, Salvatore E, Salvi F, et al. Brain structural damage in Friedreich's ataxia. *J Neurol Neurosurg Psychiatry*. 2008;79(1):82–5.
- Burk K, Malzig U, Wolf S, Heck S, Dimitriadis K, Schmitz-Hubsch T, et al. Comparison of three clinical rating scales in Friedreich ataxia (FRDA). *Mov Disord*. 2009;24(12):1779–84.
- Schmitz-Hubsch T, du Montcel ST, Baliko L, Berciano J, Boesch S, Depondt C, et al. Scale for the assessment and rating of ataxia: development of a new clinical scale. *Neurology*. 2006;66(11):1717–20.
- Diedrichsen J. A spatially unbiased atlas template of the human cerebellum. *NeuroImage*. 2006;33(1):127–38.
- Diedrichsen J, Balsters JH, Flavell J, Cussans E, Ramnani N. A probabilistic MR atlas of the human cerebellum. *NeuroImage*. 2009;46(1):39–46.
- Ashburner J, Friston KJ. Voxel-based morphometry—the methods. *NeuroImage*. 2000;11(6):805–21.
- Ashburner J, Friston KJ. Unified segmentation. *NeuroImage*. 2005;26(3):839–51.
- Rorden C, Brett M. Stereotaxic display of brain lesions. *Behav Neurol*. 2000;12(4):191–200.
- Salimi-Khorshidi G, Smith SM, Nichols TE. Adjusting the effect of nonstationarity in cluster-based and TFCE inference. *NeuroImage*. 2011;54(3):2006–19.
- Smith SM, Nichols TE. Threshold-free cluster enhancement: addressing problems of smoothing, threshold dependence and localisation in cluster inference. *NeuroImage*. 2009;44(1):83–98.
- Winkler AM, Ridgway GR, Webster MA, Smith SM, Nichols TE. Permutation inference for the general linear model. *NeuroImage*. 2014;92:381–97.
- Diedrichsen J, Zotow E. Surface-based display of volume-averaged cerebellar imaging data. *PLoS One*. 2015;10(7):e0133402.
- Ridgway GR, Barnes J, Pepple T, Fox N, editors. Estimation of total intracranial volume: a comparison of methods. AACCAD Alzheimer's imaging consortium; Paris, France; 2011.
- Malone IB, Leung KK, Clegg S, Barnes J, Whitwell JL, Ashburner J, et al. Accurate automatic estimation of total intracranial volume: a nuisance variable with less nuisance. *NeuroImage*. 2015;104:366–72.
- Yushkevich PA, Piven J, Hazlett HC, Smith RG, Ho S, Gee JC, et al. User-guided 3D active contour segmentation of anatomical structures: significantly improved efficiency and reliability. *NeuroImage*. 2006;31(3):1116–28.
- Diedrichsen J, Maderwald S, Kuper M, Thurling M, Rabe K, Gizewski ER, et al. Imaging the deep cerebellar nuclei: a probabilistic atlas and normalization procedure. *NeuroImage*. 2011;54(3):1786–94.
- Harding IH, Corben LA, Storey E, Egan GF, Stagnitti MR, Poudel GR, et al. Fronto-cerebellar dysfunction and dysconnectivity underlying cognition in Friedreich ataxia: the IMAGE-FRDA study. *Hum Brain Mapp*. 2016;37(1):338–50.
- Stefanescu MR, Dohnalek M, Maderwald S, Thurling M, Minnerop M, Beck A, et al. Structural and functional MRI abnormalities of cerebellar cortex and nuclei in SCA3, SCA6 and Friedreich's ataxia. *Brain*. 2015;138(Pt 5):1182–97.

30. Ginestroni A, Diciotti S, Cecchi P, Pesaresi I, Tessa C, Giannelli M, et al. Neurodegeneration in Friedreich's ataxia is associated with a mixed activation pattern of the brain. A fMRI study. *Hum Brain Mapp.* 2012;33(8):1780–91.
31. Deistung A, Stefanescu MR, Ernst TM, Schlamann M, Ladd ME, Reichenbach JR, et al. Structural and functional magnetic resonance imaging of the cerebellum: considerations for assessing cerebellar ataxias. *Cerebellum.* 2016;15(1):21–5.
32. Dogan I, Tinnemann E, Romanzetti S, Mirzazade S, Costa AS, Werner CJ, et al. Cognition in Friedreich's ataxia: a behavioral and multimodal imaging study. *Ann Clin Transl Neurol.* 2016;3(8):572–87.
33. Selvadurai LP, Harding IH, Corben LA, Georgiou-Karistianis N. Cerebral abnormalities in Friedreich ataxia: a review. *Neurosci Biobehav Rev.* 2018;84:394–406.
34. Grodd W, Hulsmann E, Lotze M, Wildgruber D, Erb M. Sensorimotor mapping of the human cerebellum: fMRI evidence of somatotopic organization. *Hum Brain Mapp.* 2001;13(2):55–73.
35. Buckner RL, Krienen FM, Castellanos A, Diaz JC, Yeo BT. The organization of the human cerebellum estimated by intrinsic functional connectivity. *J Neurophysiol.* 2011;106(5):2322–45.
36. Ackermann H, Brendel B. Cerebellar contributions to speech and language. In: Hickok G, Small SL, editors. *Neurobiology of language.* Elsevier; 2016.
37. Schols L, Amoiridis G, Przuntek H, Frank G, Epplen JT, Epplen C. Friedreich's ataxia. Revision of the phenotype according to molecular genetics. *Brain.* 1997;120(Pt 12):2131–40.
38. Delatycki MB, Paris DB, Gardner RJ, Nicholson GA, Nassif N, Storey E, et al. Clinical and genetic study of Friedreich ataxia in an Australian population. *Am J Med Genet.* 1999;87(2):168–74.
39. Brendel B, Ackermann H, Berg D, Lindig T, Scholderle T, Schols L, et al. Friedreich ataxia: dysarthria profile and clinical data. *Cerebellum.* 2013;12(4):475–84.
40. Folker J, Murdoch B, Cahill L, Delatycki M, Corben L, Vogel A. Dysarthria in Friedreich's ataxia: a perceptual analysis. *Folia Phoniatr Logop.* 2010;62(3):97–103.
41. Mascaldi M. The cerebellum looks normal in Friedreich ataxia. *AJNR Am J Neuroradiol.* 2013;34(2):E22.
42. Anheim M, Tranchant C, Koenig M. The autosomal recessive cerebellar ataxias. *N Engl J Med.* 2012;366(7):636–46.
43. Jacobi H, Hauser TK, Giunti P, Globas C, Bauer P, Schmitz-Hubsch T, et al. Spinocerebellar ataxia types 1, 2, 3 and 6: the clinical spectrum of ataxia and morphometric brainstem and cerebellar findings. *Cerebellum.* 2012;11(1):155–66.
44. Koeppen AH, Davis AN, Morral JA. The cerebellar component of Friedreich's ataxia. *Acta Neuropathol.* 2011;122(3):323–30.
45. Koeppen AH, Ramirez RL, Becker AB, Feustel PJ, Mazurkiewicz JE. Friedreich ataxia: failure of GABA-ergic and glycinergic synaptic transmission in the dentate nucleus. *J Neuropathol Exp Neurol.* 2015;74(2):166–76.
46. Boddaert N, Le Quan Sang KH, Rotig A, Leroy-Willig A, Gallet S, Brunelle F, et al. Selective iron chelation in Friedreich ataxia: biologic and clinical implications. *Blood.* 2007;110(1):401–8.
47. Bonilha da Silva C, Bergo FP, D'Abreu A, Cendes F, Lopes-Cendes I, Franca MC Jr. Dentate nuclei T2 relaxometry is a reliable neuroimaging marker in Friedreich's ataxia. *Eur J Neurol.* 2014;21(8):1131–6.
48. Koeppen AH, Michael SC, Knutson MD, Haile DJ, Qian J, Levi S, et al. The dentate nucleus in Friedreich's ataxia: the role of iron-responsive proteins. *Acta Neuropathol.* 2007;114(2):163–73.
49. Koeppen AH, Ramirez RL, Yu D, Collins SE, Qian J, Parsons PJ, et al. Friedreich's ataxia causes redistribution of iron, copper, and zinc in the dentate nucleus. *Cerebellum.* 2012;11(4):845–60.
50. Harding IH, Raniga P, Delatycki MB, Stagnitti MR, Corben LA, Storey E, et al. Tissue atrophy and elevated iron concentration in the extrapyramidal motor system in Friedreich ataxia: the IMAGE-FRDA study. *J Neurol Neurosurg Psychiatry.* 2016;87:1261–3.
51. van Baarsen KM, Kleinnijenhuis M, Jbabdi S, Sotiropoulos SN, Grotenhuis JA, van Cappellen van Walsum AM. A probabilistic atlas of the cerebellar white matter. *NeuroImage.* 2016;124(Pt A):724–32.
52. Eklund A, Nichols TE, Knutsson H. Cluster failure: why fMRI inferences for spatial extent have inflated false-positive rates. *Proc Natl Acad Sci U S A.* 2016;113(28):7900–5.
53. Eklund A, Andersson M, Knutsson H. Fast random permutation tests enable objective evaluation of methods for single-subject fMRI analysis. *Int J Biomed Imaging.* 2011;2011:627947.

Web References

54. Brain and Mind Institute, University of Western Ontario, Canada. Spatially unbiased infratentorial template for normalization of cerebellum and brainstem (SUIT). <http://www.diedrichsenlab.org/imaging/suit.htm> (last accessed 14.05.)
55. Wellcome Trust Centre for Neuroimaging, London, UK. Statistical Parameter Mapping (SPM). <http://www.fil.ion.ucl.ac.uk/spm/> (last accessed 14.05.)
56. Chris Rorden's Neuropsychology Lab, University of South Carolina, USA. MRICron. <http://www.mccauslandcenter.sc.edu/cml/tools> (last accessed 14.05.)
57. Structural Brain Mapping Group, University of Jena, Germany. Voxel Based Morphometry toolbox (VBM8). <http://www.neuro.uni-jena.de/vbm/download/> (last accessed 14.05.) and <http://www.neuro.uni-jena.de/vbm/check-sample-homogeneity/> (last accessed 14.05.)
58. Center for Investigating Healthy Minds, University of Wisconsin-Madison, USA. Mean centering continuous covariates. http://www.mumford.fmripower.org/mean_centering/ (last accessed 14.05.)
59. FMRIB, Oxford, UK. FMRIB Software Library (fsl). <https://fsl.fmrib.ox.ac.uk/fsl/> (last accessed 14.05.)
60. Penn Image Computing and Science Laboratory, and Scientific Computing and Imaging Institute, University of Pennsylvania and University of Utah, USA. ITK-SNAP. <http://www.itksnap.org/pmwiki/pmwiki.php> (last accessed 14.05.)